

## Article

# Controlling the Physical Properties of Fe<sub>3</sub>O<sub>4</sub>-Immobilized Palladium Complexes towards Reusable Catalysts in the Methoxycarbonylation of 1-Hexene

Saphan O. Akiri <sup>1</sup>, Markus Schmitz <sup>2</sup>  and Stephen O. Ojwach <sup>1,\*</sup> 

<sup>1</sup> School of Chemistry and Physics, University of KwaZulu-Natal, Private Bag X01, Pietermaritzburg 3209, South Africa; akirisaphan88@gmail.com

<sup>2</sup> Fachbereich Chemie, RPTU Kaiserslautern-Landau, Erwin-Schrödinger-Str. 54, 67663 Kaiserslautern, Germany

\* Correspondence: ojwach@ukzn.ac.za

**Abstract:** This paper describes the use of immobilized palladium catalysts on Fe<sub>3</sub>O<sub>4</sub> magnetic nanoparticles (MNPs) to afford magnetically separable catalysts in the methoxycarbonylation of 1-hexene. Immobilization of homogeneous complex [Pd(L1)Cl<sub>2</sub>] (**Pd1**), where L1 = N,N′E,N,N′E)-N,N′-(3-(3-(triethoxysilyl)propyl)pentane-2,4-diylidene)dianiline, on Fe<sub>3</sub>O<sub>4</sub> MNPs at 100 °C and Pd loading of 10% (based on wt% of **Pd1**) afforded the corresponding complex [Pd1@Fe<sub>3</sub>O<sub>4</sub>] (**Pd2**) in good yields. The use of calcination temperatures of 150 °C and 200 °C produced compounds **Pd3** and **Pd4**, respectively, while Pd metal loadings (based on wt% of **Pd1**) of 5% and 15% provided complexes **Pd5** and **Pd6**, respectively. The immobilized compounds were analyzed using FT-IR spectroscopy, SEM-EDX, TEM, ICP-OES, and PXRD techniques. The surface areas and porosity of the materials were determined using nitrogen physisorption measurements and confirmed the formation of mesoporous materials, while SQUID measurements established Ms values in the range of 60.69 to 69.93 emu/g. The immobilized Pd(II) complexes catalyzed the methoxycarbonylation of 1-hexene, yielding mainly linear esters. The immobilized compounds could be recycled up to five times via magnetic separation without significant loss in catalytic activities.

**Keywords:** palladium(II); immobilization; magnetic nanoparticles; methoxycarbonylation; recycling



**Citation:** Akiri, S.O.; Schmitz, M.; Ojwach, S.O. Controlling the Physical Properties of Fe<sub>3</sub>O<sub>4</sub>-Immobilized Palladium Complexes towards Reusable Catalysts in the Methoxycarbonylation of 1-Hexene. *Processes* **2023**, *11*, 2516. <https://doi.org/10.3390/pr11092516>

Academic Editor: Albert Renken

Received: 25 July 2023

Revised: 9 August 2023

Accepted: 18 August 2023

Published: 22 August 2023



**Copyright:** © 2023 by the authors. Licensee MDPI, Basel, Switzerland. This article is an open access article distributed under the terms and conditions of the Creative Commons Attribution (CC BY) license (<https://creativecommons.org/licenses/by/4.0/>).

## 1. Introduction

The increasing demand for industrial and domestic feedstocks and products has led to the search for large-scale technologies in the syntheses of these materials [1]. While significant advances have been made in the use of various catalytic processes to produce these commodities, these have not come without costs, specifically for environmental pollution [2]. The implication is that there have been efforts in recent years to develop greener and environmentally benign catalytic processes in order to reduce waste and hazardous chemicals [3]. While homogeneous catalysts have been used due to their superior selectivity and low concentrations, their lack of recycling have made them less desirable [4]. On the other hand, heterogeneous catalysts are easily recycled, but generally show poor selectivity [4]. As such, combining the merits of homogeneous (high selectivity) and heterogeneous (recyclable) catalysts in one catalyst system is an emerging area of catalyst design. This has seen the advent of supported catalyst systems, which are expected to display both high selectivity (single-site nature), in addition to being recyclable (due to the immobilization) [5,6]. A number of immobilization strategies have been used so far, such as metal organic frameworks [7], silica supports [8,9], polymer supports [10–12], magnetic nanoparticles [13], magnetic nanohybrid decorated porous organic polymer [14], wood sourced polymers [15], and hypercrosslinked microporous polymer [16]. As opposed to other support materials (silica, polymer, clay, among others), whose separation from

the reaction mixtures is rather complex, magnetic nanoparticles as supports offer an easier separation route by simply using an external magnetic field [17].

Methoxycarbonylation is one of the most versatile carbonylation reactions in synthetic organic chemistry for the production of valuable industrial feedstocks, such as solvents and domestic products, such as detergents, perfumes, fragrances, and food additives [8,18]. Traditionally, methoxycarbonylation reactions are carried out using in situ generated homogeneous catalysts from phosphine-based ligands and palladium metal salts, such as Pd(OAc)<sub>2</sub> [19,20]. More recently, the design and well-defined palladium catalysts supported on various donor ligands have emerged. Examples include palladium(II) catalysts of N<sup>^</sup>N-donor (benzoimidazol-2-ylmethyl)amine [21], pyridinimine ligands [22], iminopyridine [23], N<sup>^</sup>P-donor 2-diphenylphosphinoaniline ligands [24], and P<sup>^</sup>P-based naphthyl(diphenyl)phosphine ligands [25].

Even though the use of heterogeneous and supported homogeneous catalysts has been widely applied in various olefin transformation reactions [26–31], surprisingly, there exist very few publications on the applications of supported metal complexes as catalysts in the methoxycarbonylation reactions. Recently, we reported that silica-immobilized palladium complexes and water-soluble palladium complexes [8,32,33] promote the methoxycarbonylation of olefins, with promising results. These supported catalysts are recyclable and could be used in up to five cycles without appreciable loss in both the catalytic activity and regioselectivity. Spurred by these previous findings, we now focus on the use of magnetic nanoparticles, with the aim of improving the separation and recyclable efficiency of the magnetically supported catalysts. In this contribution, we report the preparation of immobilized palladium complexes of beta-diimine ligand and their characterization and investigation as recyclable catalysts in the methoxycarbonylation of 1-hexene.

## 2. Results and Discussion

### 2.1. Preparation and Characterization of Magnetically Immobilized Palladium Complexes

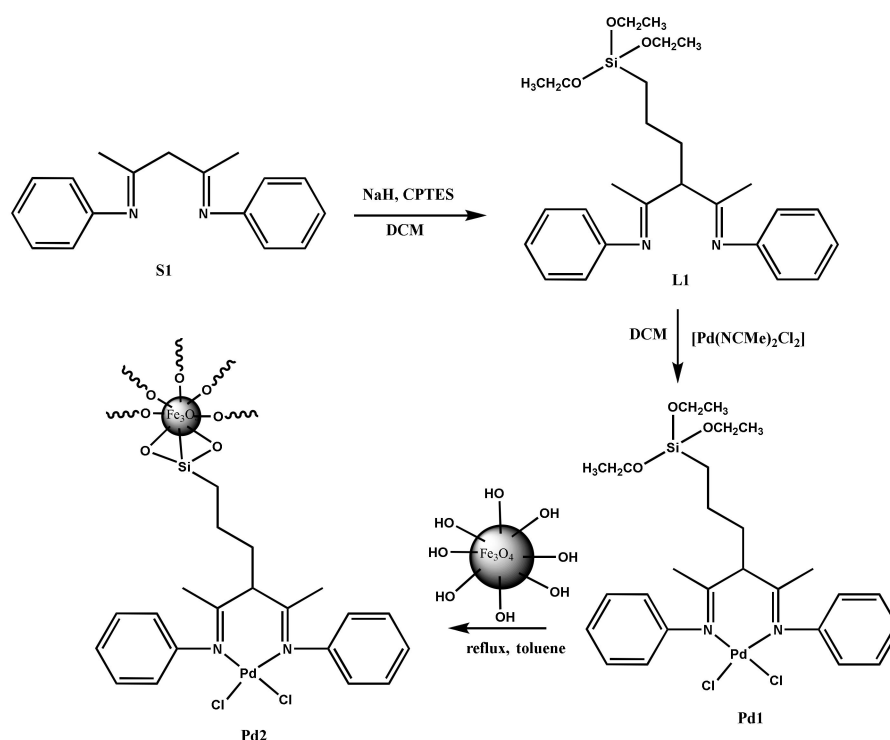
The starting beta-diimine ligand (**S1**) was prepared following the literature procedures [34] and functionalized on using 3-(chloropropyl)triethoxy silane to produce ligand N,N<sup>^</sup>E,N,N<sup>^</sup>E)-N,N<sup>^</sup>-(3-(3-(triethoxysilyl)propyl)pentane-2,4-diylidene)dianiline (**L1**) in good yields of 87% (Scheme 1). A convergent synthetic protocol was employed to prepare the immobilized homogeneous palladium complex [Pd(**L1**)Cl<sub>2</sub>] (**Pd1**) on Fe<sub>3</sub>O<sub>4</sub> magnetic nanoparticles to produce the corresponding complex [Pd1@Fe<sub>3</sub>O<sub>4</sub>] (**Pd2**) in moderate yields [35]. The same approach was employed to synthesize the analogous immobilized Pd complexes **Pd3** and **Pd4** at calcination temperatures of 150 °C and 200 °C, respectively, and **Pd5** and **Pd6** using Pd metal loadings (based on wt% of **Pd1**) of 5% and 15%, respectively (Table 1).

**Table 1.** The physical and magnetic properties of the Fe<sub>3</sub>O<sub>4</sub>-immobilized Pd(II) compounds.

Entry	Complex	Description	ICP-AES (wt%)	S <sub>BET</sub> [m <sup>2</sup> /g] <sup>a</sup>	V <sub>p</sub> [cm <sup>3</sup> /g] <sup>b</sup>	AVPD [nm] <sup>c</sup>	Ms [emu/g] <sup>d</sup>
1	<b>Pd2</b>	<b>Pd1</b> -Fe <sub>3</sub> O <sub>4</sub> @10%Pd@100 °C	1.91	44	0.1808	12.457	64.24
2	<b>Pd3</b>	<b>Pd1</b> -Fe <sub>3</sub> O <sub>4</sub> @10%Pd@150 °C	1.87	41	0.1748	12.123	63.36
3	<b>Pd4</b>	<b>Pd1</b> -Fe <sub>3</sub> O <sub>4</sub> @10%Pd@200 °C	1.92	43	0.1792	12.647	60.69
4	<b>Pd5</b>	<b>Pd1</b> -Fe <sub>3</sub> O <sub>4</sub> @5%Pd@100 °C	1.66	53	0.1946	11.346	69.93
5	<b>Pd6</b>	<b>Pd1</b> -Fe <sub>3</sub> O <sub>4</sub> @15%Pd@100 °C	2.10	41	0.1690	11.891	67.96

<sup>a</sup> BET surface area (S<sub>BET</sub>), total pore volume (V<sub>p</sub>) and micro pore volume (V<sub>micro</sub>) measured by N<sub>2</sub> physisorption.

<sup>b</sup> The V<sub>micro</sub> [cm<sup>3</sup>/g] could not be determined, confirming the mesoporous nature of the materials. <sup>c</sup> Average pore diameter (AVPD) calculated according to BJH plot. <sup>d</sup> Determined by SQUID; value of pure Fe<sub>3</sub>O<sub>4</sub> = 75.97 emu/g.



**Scheme 1.** Synthesis of Fe<sub>3</sub>O<sub>4</sub> MNPs-supported palladium(II) complex using a covalent convergent protocol.

The synthesized compounds were characterized and identified using various techniques. <sup>1</sup>H NMR spectroscopy was used to help identify ligand **L1** and its corresponding homogeneous palladium complex (**Pd1**) (Figures S1–S5). For example, the successful immobilization of **S1** to produce **L1** was established from the presence of the silane protons (1.15 ppm and 3.76 ppm) and the disappearance of β-CH (proton) at 5.2 ppm in compound **S1** (Figures S1 and S2). The successful formation of complex [Pd(**L1**)Cl<sub>2</sub>] (**Pd1**) was also confirmed by the shift in the methyl protons from 2.11 ppm in **L1** to 2.32 ppm in **Pd1** (Figure S3). FT-IR spectroscopy was also employed in the identification of the functional groups, both in homogeneous and immobilized compounds. For example, all the compounds displayed typical ν(C=N) frequencies around 1630 cm<sup>-1</sup>, pointing to the retention of the ligand upon immobilization on the magnetic iron nanoparticles (Figures S6–S8). In addition, the immobilized complex **Pd2** showed frequencies at 3341 and 583 cm<sup>-1</sup>, which can be associated with the ν(Si-OH) and ν(Fe-O), respectively (Figure S9), in good agreement with the findings of Asadi et al. of 3457 and 607 cm<sup>-1</sup>, respectively [36].

The surface morphology and elemental composition of the Fe<sub>3</sub>O<sub>4</sub>-supported complexes were analyzed using SEM-EDX and TEM. The SEM images of the Fe<sub>3</sub>O<sub>4</sub>-immobilized complex **Pd2** showed particles on non-uniform shapes with aggregation. (Figure 1). However, the darker shades of the Fe<sub>3</sub>O<sub>4</sub> MNP are visible, showing that the Pd atom and the organic ligand are well fused into the iron nanoparticle core (Figure 1). SEM-EDX was also applied for quantitative elemental analysis and mapping. From the EDX spectral data, the expected elements, Fe, Si, C, N, O, Pd, and Cl, were observed, an indication of immobilization of the complex onto the Fe<sub>3</sub>O<sub>4</sub> MNP (Figure S12). ICP-OES was employed to further determine the quantitative elemental compositions of the compounds (Table 1). From the data, the palladium loadings in all the materials were in the range from 1.91 to 2.10%. The current results compare well with the literature reports of Veisi et al. of 2.19% [37]. Indeed, higher Pd loadings were accompanied by higher Pd metal content. For example, compounds **Pd5** (5% Pd), **Pd2** (10% Pd), and **Pd6** (15% Pd) exhibited Pd metal contents (wt%) of 1.68, 1.91, and 2.10, respectively (Table 1; entries 1, 4, and 5). TEM was further used in evaluating the morphology and particle size of the compounds. From Figure 2, both the pure Fe<sub>3</sub>O<sub>4</sub>

and compound **Pd2** showed spherical particles of different sizes. Analysis of the particle size for compound **Pd2** using imageJ plot (Figure S13) revealed that the average particle size was 10.33 nm, which is an indication of the mesoporous nature of the immobilized palladium materials.

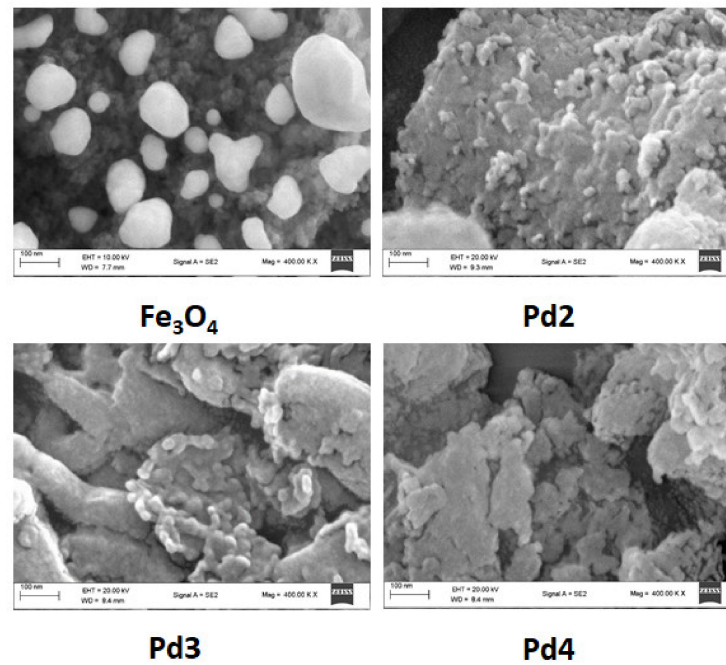


**Figure 1.** SEM images of pure  $\text{Fe}_3\text{O}_4$  MNPs and the immobilized complexes **Pd2**, **Pd3**, and **Pd4** showing quasi-spherical particles and varied degrees of agglomeration.

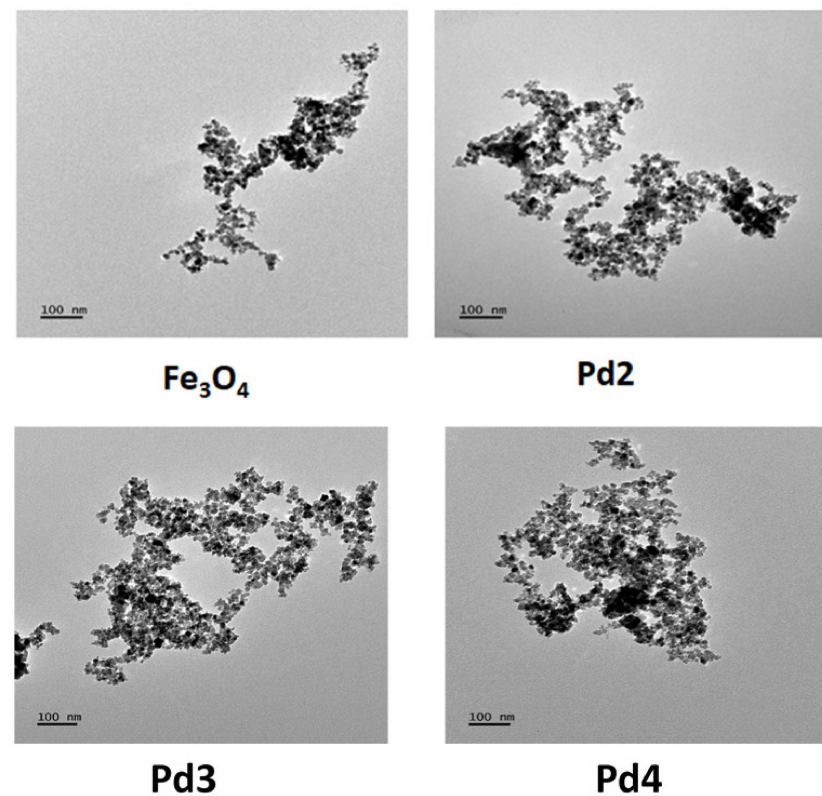


**Figure 2.** TEM images of pure  $\text{Fe}_3\text{O}_4$  MNPs and the corresponding immobilized materials **Pd2**, **Pd3**, and **Pd4** showing quasi-spherical particles.

The magnetic properties of the  $\text{Fe}_3\text{O}_4$  MNP-immobilized Pd(II) materials were also studied using a superconducting quantum interference device (SQUID), as depicted in Figure 3 and Table 1. The saturation magnetization of the pure  $\text{Fe}_3\text{O}_4$  MNP of 75.97 emu/g was expectedly higher than those of the immobilized materials in the range of 60.69 emu/g to 69.93 emu/g (Table 1, entries 1–4). The drop in superparamagnetic properties is understandable from the incorporation of the diamagnetic Pd(II) atoms into the  $\text{Fe}_3\text{O}_4$  MNP core [38]. Indeed, compound **Pd5**, with the lowest palladium loadings of 5%, displayed the highest  $M_s$  value of 69.93 (Table 1, entry 5). The higher calcination temperature of 200 °C resulted in a significantly lower  $M_s$  value of 60.69 emu in compound **Pd4**, compared to the  $M_s$  value of 64.24 emu at 100 °C in compound **Pd2**. This trend may be associated with the greater damage of the magnetic field and alignments of the compounds at higher temperatures [39]. It is important to note that all the saturation magnetization values are sufficient to facilitate efficient catalysis recovery [40].

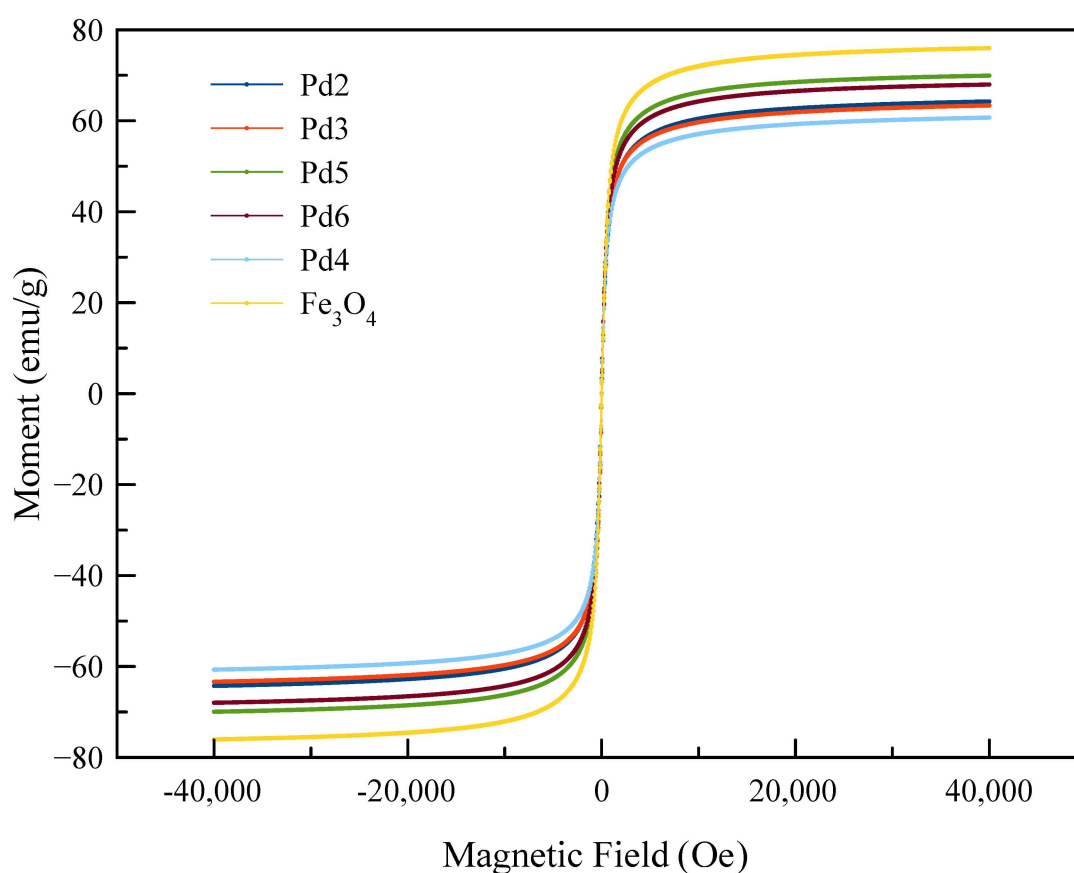


**Figure 3.** Room-temperature magnetization curves of pure  $\text{Fe}_3\text{O}_4$  magnetic nanoparticles and the supported palladium complexes.

The thermal properties of the materials were studied using TGA and decomposition profiles acquired in the temperature range between 0 to 900 °C (Figures S14–S18). The compounds generally showed three specific phases of decomposition. The initial phase of decomposition was observed between 0 and 200 °C. This first decomposition phase can be associated with the loss of the moisture content of the materials. The next phase of the decomposition was observed between 200 and 400 °C, which can be connected to the elimination of the compound's organic core. The last phase then proceeded through to 900 °C.

The specific surface areas of the  $\text{Fe}_3\text{O}_4$ -immobilized palladium compounds were determined by nitrogen physisorption measurements, according to Brunauer, Emmett, Teller (BET), while the porosity were determined using the Barrett, Joyner, Halenda (BJH)

method (Table 1 and Figures S19–S23). The adsorption–desorption isotherms show type II adsorption, with an H3-type hysteresis loop and indication of the presence of mesoporous materials (Figure S19). The pore size distribution (according to BJH) for compounds **Pd2–Pd6** depicts large distributions, with the majority of the particles showing particle sizes within the 10 nm range (Figure S20). The specific surface areas were found to be dependent on the palladium loadings and content, with higher loadings having a negative impact. For example, while compound **Pd5** with 5% Pd loading exhibited a surface area of 53 m<sup>2</sup>/g, compound **Pd6** with 15% Pd palladium loading exhibited a lower specific area of 41 m<sup>2</sup>/g (Table 1, entries 4 and 5). Lower surface areas at higher metal contents have been observed and associated with occupation of the metal of the support cavities by the metal atoms [41]. This trend is concomitant with the higher total pore volumes of 0.1946 cm<sup>3</sup>/g for compound **Pd5** (5%Pd) compared to the pore volume of 0.1690 cm<sup>3</sup>/g recorded for **Pd6** (15%Pd) (Table 1, entries 4 and 5).

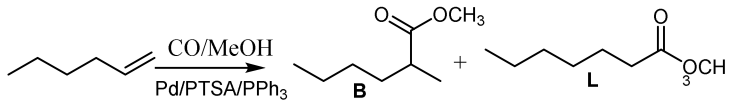
The crystallinity and phase composition of the compounds were explored using powder X-ray diffraction (PXRD), as shown in Figure S21. From the diffraction patterns, six characteristic signals of Fe<sub>3</sub>O<sub>4</sub> nanomaterial are observed at 2θ of 35.3°, 41.7°, 50.8°, 63.3°, 67.7°, and 74.7°, assigned to the hkl values of (220), (311), (400), (422), (511), and (440), respectively, consistent with the cubic spinel structure [42,43]. Upon immobilization, the diffraction peaks were retained, establishing the retention of the crystalline phase of the Fe<sub>3</sub>O<sub>4</sub> nanomaterial. The additional diffraction peaks at 18.5°, 22.8°, and 30.2° affirm the presence of the Pd(0) nanoparticles on the Fe<sub>3</sub>O<sub>4</sub> nanomaterial surface [44].

## 2.2. Methoxycarbonylation Reactions

### 2.2.1. Optimization Experiments of the Methoxycarbonylation Reactions

The immobilized palladium complexes (**Pd2–Pd6**) were investigated for their ability to catalyze the methoxycarbonylation reactions using 1-hexene in the presence of *para*-toluene sulfonic acid (PTSA), PPh<sub>3</sub>, CO, and methanol (Table 2). First, the reaction conditions were optimized using homogeneous complex (**Pd1**), as contained in Tables S1 and S2. The use of homogeneous complex **Pd1** also allowed us to compare the behaviors of non-immobilized and immobilized systems. The optimized conditions of the Pd:hexene ratio of 1:400, time of 24 h, temp of 100 °C, and pressure of 60 bar were established, producing percentage yields of 93% and TON of 372 (Table S1, entry 6). Further optimization reactions established the optimum Pd:PPh<sub>3</sub>:PTSA ratios of 1:2:20 to produce percentage yields of 98% and TON of 392 (Table 2, entry 4). Analysis of the products showed the formation of both branched and linear esters, as depicted in Table 2 (Figures S22 and S23). These optimized conditions were, thus, used to investigate the Fe<sub>3</sub>O<sub>4</sub> complexes (**Pd2–Pd6**) in the methoxycarbonylation reaction of 1-hexene.

**Table 2.** Effect of palladium loading on material property and catalytic performance <sup>a</sup>.



Entry	Complex	[Pd] <sup>b</sup> (wt%)	SBET <sup>c</sup> [m <sup>2</sup> /g]	TPV <sup>c</sup> [cm <sup>3</sup> /g]	Yield <sup>d</sup> (%)	B/L <sup>d</sup> (%)	TON <sup>e</sup>
1	<b>Pd2</b>	1.91	44	0.1808	81	33/67	324
2	<b>Pd5</b>	1.66	53	0.1946	75	33/67	334
3	<b>Pd6</b>	2.10	41	0.1690	77	32/68	280

<sup>a</sup> Reaction conditions: Solvent, methanol/toluene (40 mL); Hexene (0.5 mL); Pd (0.06 g); Pd:PPh<sub>3</sub>:PTSA ratio, 1:2:30; time, 24 h; temp, 100 °C; Pressure, 60 bar. <sup>b</sup> Determined by ICP-OES; <sup>c</sup> surface area and total pore volume (V<sub>p</sub>) measured by N<sub>2</sub> physisorption; <sup>d</sup> Determined by GC; <sup>e</sup> TON = (mol. prod./mol.Pd), calculated based on moles of Pd and moles of product formed.

### 2.2.2. Investigation of the Role of Palladium Loading on the Catalytic Behavior

Using the optimized conditions, we first explored the catalytic behavior of the immobilized palladium materials synthesized at different palladium loadings using complexes **Pd2** (10%), **Pd5** (5%), and **Pd6** (15%). From Table 2, it can be observed that the palladium loading had a significant impact on the catalytic performance of the synthesized compounds. To illustrate, palladium loading of 5% (**Pd5**) and 10% (**Pd2**) produced percentage yields of 75% and 81%, respectively (Table 2, entries 1 and 2). However, a further increase in the palladium loading to 15% (**Pd6**) saw a decrease in percentage yield to 77% (Table 2, entry 3). The enhanced catalytic performance with an increase in catalyst loading from 5% to 10% may be associated to the higher number of active Pd sites in **Pd2** as compared to **Pd5**, in good agreement with the % wt/g of Pd of 1.91 and 1.61 in catalysts **Pd2** and **Pd5**, respectively (Table 2, entries 1 and 2). Separately, the diminished percentage yield reported for **Pd6** could arise from possible catalyst aggregation [45,46]. This observation is augmented by the lower specific surface area of complex **Pd6** of 41 m<sup>2</sup>/g compared to the surface area of 53 m<sup>2</sup>/g exhibited by complex **Pd5** (Table 2, entries 2 and 3). As expected, the TONs followed an opposite trend, where complex **Pd5**, with the lowest Pd loading, recorded the highest TON (Figure S24). In terms of ester distributions, it is worth noting that no observable impact on the formation of linear esters (67–68%) was observed with the changes in palladium content. This is plausible from the viewpoint of regioselectivity being sterically controlled [47].

### 2.2.3. Role of Calcination Temperature on Material Property and Catalytic Activity

The comparative catalytic performance of the materials prepared at different calcination temperatures, **Pd2** (100 °C), **Pd3** (150 °C), and **Pd4** (200 °C), was also studied (Table 2). It was also observable that an increase in calcination temperatures resulted in lower catalytic activities of the materials. For instance, complexes **Pd2** (calcined at 100 °C) and **Pd4** (200 °C) produced percentage yields of 81% and 72%, respectively (Table 3, entries 1 vs. 3). A more detailed analysis of the data shows that catalyst **Pd4** (calcined at 200 °C) had the lowest total pore volume and specific surface area of 0.1748 cm<sup>3</sup>/g and 41 m<sup>2</sup>/g, respectively (Table 3, entry 3). These have the overall effects of minimizing substrate/catalyst interactions, consistent with the lower catalytic activities observed for **Pd4** [48].

**Table 3.** Effect of calcination temperature of the materials on their catalytic performance <sup>a</sup>.

Entry	Complex	Temp <sup>b</sup>	SBET [m <sup>2</sup> /g] <sup>c</sup>	TPV [cm <sup>3</sup> /g] <sup>c</sup>	Yield (%) <sup>d</sup>	B/L (%) <sup>d</sup>	TON <sup>e</sup>
1	<b>Pd2</b>	100	44	0.1808	81	33/67	324
2	<b>Pd3</b>	150	43	0.1792	77	30/70	308
3	<b>Pd4</b>	200	41	0.1748	72	32/68	288

<sup>a</sup> Reaction conditions: Solvent, methanol/toluene (40 mL); Pd, hexene ratio, 1:400; time, 24 h; temp, 100 °C; Pressure, 60 bar. <sup>b</sup> calcination temperature of the catalyst; <sup>c</sup> surface area and total pore volume (Vp) measured by N<sub>2</sub> physisorption; <sup>d</sup> Determined by GC; <sup>e</sup> TON = (mol. product/mol.Pd).

### 2.2.4. Recycling of the F<sub>3</sub>O<sub>4</sub>-Immobilized Palladium Catalysts

The ultimate goal of this work was to establish if these Fe<sub>3</sub>O<sub>4</sub> MNP-immobilized palladium complexes could be recycled by the use of an external magnet in these methoxy-carbonylation reactions. Thus, complex **Pd2** was recycled four times as shown in, producing Figure 4. From the recycling data, even though catalyst **Pd2** remained active in the subsequent runs, an appreciable drop in percentage yields from 81% to 62% in the fifth run was recorded (Figure 4). This represents a drop of about 19% between the initial and fifth cycles. On a positive note, the regioselectivity of complex **Pd2** remained invariant throughout the recycling experiments, giving linear esters of 67% and 68% in the original and fifth runs (Figure 4). Our attention then shifted to the understanding of the reasons leading to the loss in catalytic activities. We then analyzed the fresh and recovered catalyst materials, using TEM (Figure 5) and ICP-OES to establish any structural changes to the

catalyst and/or leaching of the Pd active species during the recycling experiments. From the TEM analyses, the fresh catalyst was observed to have monodispersed particles on the surface, while substantial agglomeration of particles was observed on the spent catalyst (fifth run), evident from the reduced dispersion of the **Pd2** particles (Figure 5B). Thus, the change in material structure may explain the observed loss of catalytic viability in subsequent experiments [49]. This is also plausible considering the possible reduction of the Pd<sup>2+</sup> species in the fresh material to a Pd(0), believed to be the active species in these immobilized catalysts [8], and is consistent with the PXRD data. In addition, ICP-OES data revealed a significant decline in the Pd content from 1.91% to 1.31% in the fresh and used materials, respectively. However, hot filtration experiments did not result in any catalytic activity. The lack of catalytic activity of the filtrate could be due to very low concentrations of the Pd active species (threshold not met), but may not necessarily rule out the possibility of Pd metal leaching. Thus, it is plausible to argue that the diminished catalytic performance of complex **Pd2** in the recycling studies may arise from changes in the material structure and loss of the active Pd species [50].

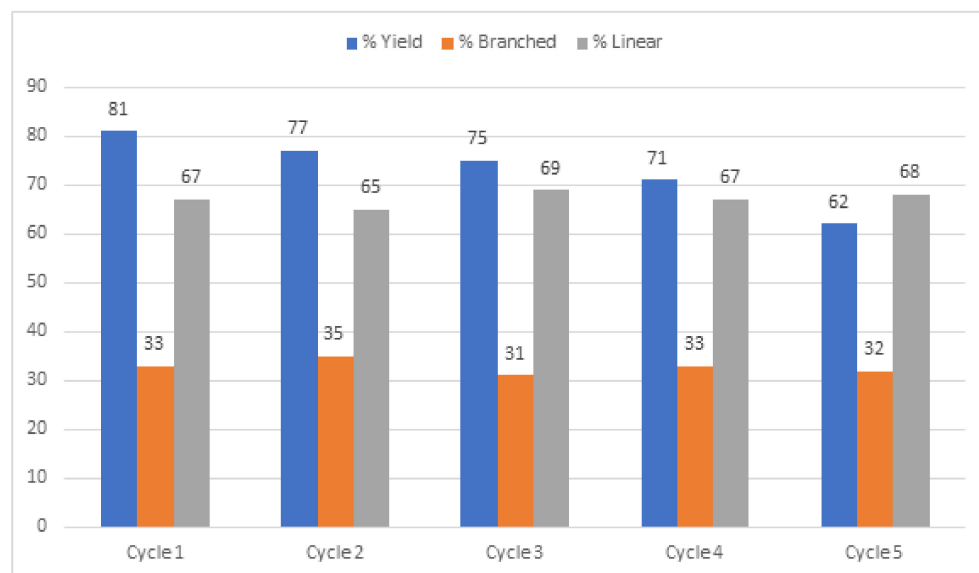


**Figure 4.** Recycling experiments data of complex **Pd2** in the methoxycarbonylation of 1-hexene.

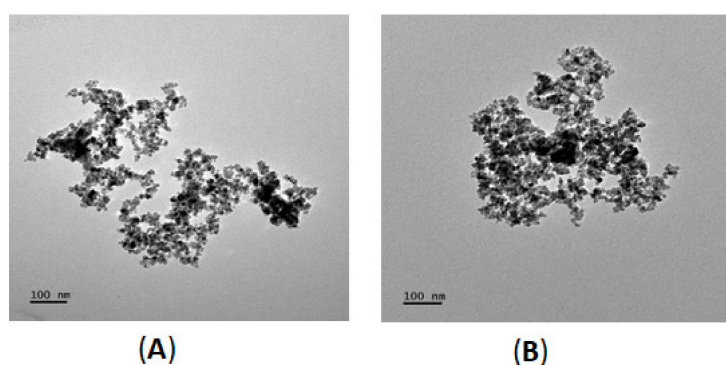


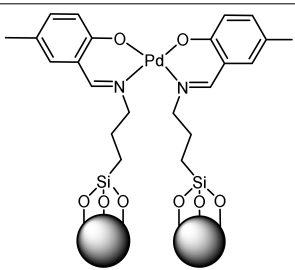
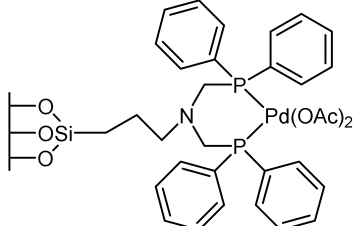
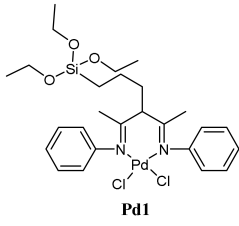
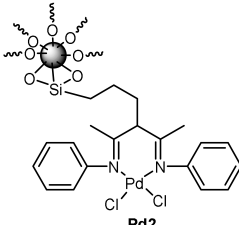
**Figure 5.** TEM images showing fresh catalyst **Pd2** (A) and used catalysts (B), showing monodispersed-to-agglomerated particles, respectively.

#### 2.2.5. Comparison of Catalytic Activities of Complex **Pd2** to the Reported Supported Systems

Finally, we compared the catalytic activities of the Fe<sub>3</sub>O<sub>4</sub>-immobilized palladium complex **Pd2** with its homogeneous (**Pd1**) counterpart and other reported immobilized systems (Table 4). From Table 4, the immobilization of complex **Pd1** on Fe<sub>3</sub>O<sub>4</sub> to produce

complex **Pd2** results in lower yields from 98% to 81%, respectively (Table 4, entries 4 and 5). Superior catalytic activities of homogeneous catalysts when compared to supported systems are known and associated with low solubility of the supported catalysts [51]. More significantly, the regioselectivity of catalyst **Pd2** was comparable to that of the homogeneous analogue **Pd1**, producing linear esters of 67% and 63% respectively (Table 2, entry 1 and Table S2, entry 4) When compared to other supported catalysts reported in the literature, complex **Pd2** falls within the generally observed catalytic activities and number of cycles (Table 4; entries 1–3 and 5). For example, the percentage yields of 81% reported for **Pd2** compare favorably with the values of 78% and 82% reported for the silica-immobilized N<sup>+</sup>O<sup>-</sup> and P<sup>+</sup>P<sup>-</sup>-donor Pd complexes in the methoxycarbonylation of 1-hexene [8] and 1-decene [52], respectively (Table 4, entries 1–2).

**Table 4.** Comparison of current palladium with reports systems.

Entry	Catalyst	Support	Substrate	% Yield (t)	Cycles	Reference
1		Silica	1-hexene	78 (24 h)	4	[8]
2		Silica	1-decene	82 (22 h)	4	[52]
3	Pd/PPh <sub>3</sub> @POP POP = porous organic polymer	Polymer	Styrene	97 (5 h)	5	[53]
4	 <b>Pd1</b>	-	1-hexene	98 (24 h)	-	This work
5	 <b>Pd2</b>	Fe <sub>3</sub> O <sub>4</sub>	1-hexene	81 (24 h)	5	This work

### 3. Conclusions

In summary, we have prepared five different N<sup>+</sup>N<sup>-</sup>-donor palladium complexes immobilized on Fe<sub>3</sub>O<sub>4</sub> magnetic nanoparticles. The physical properties of the materials were manipulated by variation of the Pd content and calcination temperatures. A range of spectroscopic and physical measurements, such as FT-IR, SEM-EDX, TEM, ICP-OES, PXRD, N<sub>2</sub> physisorption, and SQUID, were used to characterize the materials. In all cases,

mesoporous materials with sufficient magnetic susceptibilities were formed. All of the  $\text{Fe}_3\text{O}_4$ -immobilized materials were active in the methoxycarbonylation of 1-hexene to produce mainly linear esters. The catalytic performance of the materials was influenced largely by their Pd contents and specific surface areas. The immobilized catalysts were reused up to five times, with an appreciable drop in catalytic activities in the fifth run. Post-catalyst analyses point to changes in the material morphology and loss of the active Pd species during the recycling experiments.

## 4. Experimental Section

### 4.1. Instrumentation and General Materials

The chemicals aniline (99.5%), sodium hydride (95%), sodium carbonate, and palladium dichloride (95.5%), 3-chloropropyl triethoxy silane (98.5%), SBA-15, and MCM-41 were obtained from Sigma-Aldrich.  $\text{Fe}_3\text{O}_4$  MNPs were prepared according to reported protocols [54]. Transition Electron Microscopy, TEM (JEOL JEM, 1400 model) set at 200 kV accelerating voltage was employed to record the TEM images. The compounds were sonicated in ethanol prior to mounting on carbon-coated copper grids. The particle morphology and particles sizes were analyzed using a scanning electron microscope (SEM) model, ZEISS EVO LS15, working at an accelerating voltage of 20 kV. The qualitative elemental contents of the immobilized palladium(II) materials were acquired on an Oxford EDX detector. The powder X-ray diffraction spectral data were obtained on an XPERT-PRO XRD instrument with  $\text{CuK}\alpha$  radiation set at  $4.01$  to  $89.9^\circ$  as the  $2\theta$  range. Elemental composition and mapping were recorded on a Varian 720-ES inductively coupled plasma atomic emission spectroscopy (ICP-AES) suited with an ICP Expert II software. Nitrogen physisorption measurements were performed on the BELSORP MAX from Microtrac Retzsch. Data evaluation according to Brunauer, Emmett, Teller (BET) and Barrett, Joyner, Halenda (BJH) was carried out with the software BELmaster version 7.3.2.0. The samples were activated in a vacuum for 20 h at  $130^\circ\text{C}$  prior to the measurements. Thermogravimetric analyses were acquired on a Perkin-Elmer TGA 4000 instrument equipped with Pyris software at  $50$ – $900^\circ\text{C}$  with a  $10^\circ\text{C}/\text{min}$  heating rate. Magnetic susceptibility measurements were carried out with a Quantum Design MPMS3 Evercool SQUID magnetometer equipped with a 7 Tesla magnet at 300 K, with variable applied dc magnetic fields between  $-4$  T ( $-40,000$  Oe) and 4 T (40,000 Oe) in DC mode.

### 4.2. Preparation of the $\text{Fe}_3\text{O}_4$ Magnetic Nanoparticle-Immobilized Palladium Compounds

#### 4.2.1. Synthesis of Complex $[\text{Pd1-Fe}_3\text{O}_4@10\%\text{Pd}@100^\circ\text{C}]$ (Pd2)

To a mixture of complex  $[\text{Pd}(\mathbf{L1})\text{Cl}_2]$ , **Pd1** (0.10 g, 0.16 mmol), where  $\mathbf{L1} = \text{N}_2\text{N}'\text{E}_2\text{N}_2\text{N}'\text{E}$ - $\text{N}_2\text{N}'$ -(3-(3-(triethoxysilyl)propyl)pentane-2,4-diyldiene)dianiline, in toluene (10 mL) was added  $\text{Fe}_3\text{O}_4$  (1.00 g). The resultant mixture was then sonicated for 20 min and further refluxed for 12 h. The material was cooled to room temperature and filtered to obtain a yellow solid. The solid was washed three times with ethanol (3 mL) and dried in the oven overnight to produce **Pd2** as a brown solid yield = 0.80 g (72%). IR  $\nu_{\text{max}}/\text{cm}^{-1}$ :  $\nu(\text{C}=\text{N}) = 1597$ ,  $\nu(\text{Si}-\text{O}) = 1053$ ,  $\nu(\text{Si}-\text{OH}) = 3341$ ,  $\nu(\text{Fe}-\text{O}) = 583$ . The compound was calcined at  $150^\circ\text{C}$  and  $200^\circ\text{C}$  to yield **Pd3** and **Pd4**, respectively.

#### 4.2.2. Synthesis of $[\text{Pd1-Fe}_3\text{O}_4@5\%\text{Pd}@100^\circ\text{C}]$ (Pd5)

Complex **Pd5** was prepared according to the method described for **Pd2** by using **Pd1** (0.05 g, 0.08 mmol) and  $\text{Fe}_3\text{O}_4$  (1.00 g). Yield = 0.82 g (78%). IR  $\nu_{\text{max}}/\text{cm}^{-1}$ :  $\nu(\text{C}=\text{N}) = 1593$ ,  $\nu(\text{Si}-\text{O}) = 1024$ ,  $\nu(\text{Si}-\text{OH}) = 3346$ ,  $\nu(\text{Fe}-\text{O}) = 596$ .

#### 4.2.3. Synthesis of $[\text{Pd1-Fe}_3\text{O}_4@15\%\text{Pd}@100^\circ\text{C}]$ (Pd6)

Complex **Pd6** was prepared in a similar way to complex **Pd2** by using **Pd1** (0.15 g, 0.24 mmol) and  $\text{Fe}_3\text{O}_4$  (1.00 g). Yield = 0.84 g (73%). IR  $\nu_{\text{max}}/\text{cm}^{-1}$ :  $\nu(\text{C}=\text{N}) = 1596$ ,  $\nu(\text{Si}-\text{O}) = 1024$ ,  $\nu(\text{Si}-\text{OH}) = 3375$ ,  $\nu(\text{Fe}-\text{O}) = 607$ .

**Supplementary Materials:** The following supporting information can be downloaded at: <https://www.mdpi.com/article/10.3390/pr11092516/s1>, Figures S1–S5: NMR spectra; Figures S6–S11: FT-IR spectra; Figure S12: EDX spectrum of Pd2; Figure S13: Image J plot showing the particle size distribution for Pd2; Figures S14–S18: TGA thermograms; Figure S19: N<sub>2</sub> adsorption-desorption isotherms; Figure S20: Pore-size distribution graphs; Figure S21: PXRD patterns; Figures S22 and S23: GC and GC spectra; Figure S24: Plot of TON and %Yield vs catalyst loading; Table S1: Optimization methoxycarbonylation data; Table S2: Optimization of the Pd:PPh<sub>3</sub> and Pd:PTSA ratios and CO pressure using complex Pd1<sup>a</sup>

**Author Contributions:** S.O.A. conceptualization, methodology, data analyses, writing original draft; M.S. methodology, validation, software, and editing. S.O.O. conceptualization, funding and resources, supervision, writing review. All authors have read and agreed to the published version of the manuscript.

**Funding:** This research was funded by DST-NRF (South Africa) Centre of Excellence in Catalysis (c\*change) grant number [OLE-11.3-UKZN], DFG, grant number [INST 248/266-1 FUGG] and SFB, grant number [TRR-88].

**Data Availability Statement:** Not applicable.

**Acknowledgments:** The authors would like to thank Werner R. Thiel for hosting SO during his sabbatical at RPTU. Benjamin Heider and Alina Ouissa (RPTU) are acknowledged for performing thermogravimetric and nitrogen physisorption measurements.

**Conflicts of Interest:** The authors declare no conflict of interest.

## References

1. Hagen, J. *Industrial Catalysis: A Practical Approach*; John Wiley & Sons: Hoboken, NJ, USA, 2015.
2. Centi, G.; Perathoner, S. Catalysis and sustainable (green) chemistry. *Catal. Today* **2003**, *77*, 287–297. [[CrossRef](#)]
3. Dunn, P.J. The importance of green chemistry in process research and development. *Chem. Soc. Rev.* **2012**, *41*, 1452–1461. [[CrossRef](#)] [[PubMed](#)]
4. Hübner, S.; de Vries, J.G.; Farina, V. Why does industry not use immobilized transition metal complexes as catalysts? *Adv. Synth. Catal.* **2016**, *358*, 3–25. [[CrossRef](#)]
5. Piermatti, O.; Abu-Reziq, R.; Vaccaro, L. Strategies to Immobilized Catalysts: A Key Tool for Modern Chemistry. *Catal. Immobil. Methods Appl.* **2020**, *18*, 1–22.
6. Gürsel, I.V.; Noël, T.; Wang, Q.; Hessel, V. Separation/recycling methods for homogeneous transition metal catalysts in continuous flow. *Green Chem.* **2015**, *17*, 2012–2026. [[CrossRef](#)]
7. Isaeva, V.I.; Eliseev, O.L.; Chernyshev, V.V.; Bondarenko, T.N.; Vergun, V.V.; Kapustin, G.I.; Lapidus, A.L.; Kustov, L.M. Palladium nanoparticles embedded in MOF matrices: Catalytic activity and structural stability in iodobenzene methoxycarbonylation. *Polyhedron* **2019**, *158*, 55–64. [[CrossRef](#)]
8. Akiri, S.O.; Ojwach, S.O. Synthesis of MCM-41 Immobilized (Phenoxy) Imine Palladium (II) Complexes as Recyclable Catalysts in the Methoxycarbonylation of 1-Hexene. *Catalysts* **2019**, *9*, 143. [[CrossRef](#)]
9. Mukhopadhyay, K.; Sarkar, B.R.; Chaudhari, R.V. Anchored Pd complex in MCM-41 and MCM-48: Novel heterogeneous catalysts for hydrocarboxylation of aryl olefins and alcohols. *J. Am. Chem. Soc.* **2002**, *124*, 9692–9693. [[CrossRef](#)]
10. Beletskaya, I.; Ganina, O. Hydroxy- and alkoxy-carbonylation of aryl iodides catalyzed by polymer-supported palladium, Reaction Kinetics. *Mech. Catal.* **2010**, *99*, 1–4.
11. Chen, X.; Zhu, H.; Wang, T.; Li, C.; Yan, L.; Jiang, M.; Liu, J.; Sun, X.; Jiang, Z.; Ding, Y. The 2V-P, N polymer supported palladium catalyst for methoxycarbonylation of acetylene. *J. Mol. Catal. A Chem.* **2016**, *414*, 37–46. [[CrossRef](#)]
12. Doherty, S.; Knight, J.G.; Betham, M. The first insoluble polymer-bound palladium complexes of 2-pyridyldiphenylphosphine: Highly efficient catalysts for the alkoxy-carbonylation of terminal alkynes. *Chem. Commun.* **2006**, *1*, 88–90. [[CrossRef](#)] [[PubMed](#)]
13. Dutta, B.; Omar, S.; Natour, S.; Abu-Reziq, R. Palladium nanoparticles immobilized on magnetic nanoparticles: An efficient semi-heterogeneous catalyst for carbonylation of aryl bromides. *Catal. Commun.* **2015**, *61*, 31–36. [[CrossRef](#)]
14. Dhanalaxmi, K.; Singuru, R.; Mondal, S.; Bai, L.; Reddy, B.M.; Bhaumik, A.; Mondal, J. Magnetic nanohybrid decorated porous organic polymer: Synergistic catalyst for high performance levulinic acid hydrogenation. *ACS Sustain. Chem. Eng.* **2017**, *5*, 1033–1045. [[CrossRef](#)]
15. Negui, M.; Zhang, Z.; Foucher, C.; Guénin, E.; Richel, A.; Jeux, V.; Terrasson, V. Wood-sourced polymers as support for catalysis by group 10 transition metals. *Processes* **2022**, *10*, 345. [[CrossRef](#)]
16. Molla, R.A.; Bhanja, P.; Ghosh, K.; Islam, S.S.; Bhaumik, A.; Islam, S.M. Pd nanoparticles decorated on hypercrosslinked microporous polymer: A highly efficient catalyst for the formylation of amines through carbon dioxide fixation. *ChemCatChem* **2017**, *9*, 1939–1946. [[CrossRef](#)]

17. Yang, C.; Wu, J.; Hou, Y. Fe<sub>3</sub>O<sub>4</sub> nanostructures: Synthesis, growth mechanism, properties and applications. *Chem. Commun.* **2011**, *47*, 5130–5141. [[CrossRef](#)] [[PubMed](#)]
18. Akiri, S.O.; Ojwach, S.O. Methoxycarbonylation of olefins catalysed by homogeneous palladium (II) complexes of (phenoxy) imine ligands bearing alkoxy silane groups. *Inorg. Chim. Acta* **2019**, *489*, 236–243. [[CrossRef](#)]
19. Williams, D.B.G.; Shaw, M.L.; Green, M.J.; Holzappel, C.W. Aluminum triflate as a highly active and efficient nonprotic cocatalyst in the palladium—Catalyzed methoxycarbonylation reaction. *Angew. Chem.* **2008**, *120*, 570–573. [[CrossRef](#)]
20. Vieira, T.O.; Green, M.J.; Alper, H. Highly regioselective anti-markovnikov palladium-borate-catalyzed methoxycarbonylation reactions: Unprecedented results for aryl olefins. *Org. Lett.* **2006**, *8*, 6143–6145. [[CrossRef](#)]
21. Tshabalala, T.A.; Ojwach, S.O.; Akerman, M.A. Palladium complexes of (benzoimidazol-2-ylmethyl) amine ligands as catalysts for methoxycarbonylation of olefins. *J. Mol. Catal. A Chem.* **2015**, *406*, 178–184. [[CrossRef](#)]
22. Bianchini, C.; Lee, H.M.; Mantovani, G.; Meli, A.; Oberhauser, W. Bis-alkoxycarbonylation of styrene by pyridinimine palladium catalysts. *New J. Chem.* **2002**, *26*, 387–397. [[CrossRef](#)]
23. Ngcobo, N.L.; Akiri, S.O.; Ogwenso, A.O.; Ojwach, S.O. Structural elucidation of chiral (imino) pyridine/phosphine palladium (II) complexes and their applications as catalysts in methoxycarbonylation of styrene. *Polyhedron* **2021**, *203*, 115243. [[CrossRef](#)]
24. Abarca, G.; Brown, K.; Moya, S.A.; Bayón, J.C.; Aguirre, P.A. Methoxycarbonylation of Styrene Using a New Type of Palladium Complexes Bearing P, N-donor Ligands as Catalysts. *Catal. Lett.* **2015**, *145*, 1396–1402. [[CrossRef](#)]
25. Zolezzi, S.; Moya, S.A.; Valdebenito, G.; Abarca, G.; Parada, J.; Aguirre, P. Methoxycarbonylation of olefins catalyzed by palladium (II) complexes containing naphthyl (diphenyl) phosphine ligands. *Appl. Organomet. Chem.* **2014**, *28*, 364–371. [[CrossRef](#)]
26. Polshettiwar, V.; Molnár, Á. Silica-supported Pd catalysts for Heck coupling reactions. *Tetrahedron* **2007**, *63*, 6949–6976. [[CrossRef](#)]
27. Díaz-Sánchez, M.; Díaz-García, D.; Prashar, S.; Gómez-Ruiz, S. Palladium nanoparticles supported on silica, alumina or titania: Greener alternatives for Suzuki–Miyaura and other C–C coupling reactions. *Environ. Chem. Lett.* **2019**, *17*, 1585–1602. [[CrossRef](#)]
28. Camacho-Bunquin, J.; Ferrandon, M.; Sohn, H.; Yang, D.; Liu, C.; Leon, P.A.I.-D.; Perras, F.A.; Pruski, M.; Stair, P.C.; Delferro, M. Chemoselective hydrogenation with supported organoplatinum (IV) catalyst on Zn (II)-modified silica. *J. Am. Chem. Soc.* **2018**, *140*, 3940–3951. [[CrossRef](#)] [[PubMed](#)]
29. Gong, Y.; Li, M.; Li, H.; Wang, Y. Graphitic carbon nitride polymers: Promising catalysts or catalyst supports for heterogeneous oxidation and hydrogenation. *Green Chem.* **2015**, *17*, 715–736. [[CrossRef](#)]
30. Jayamani, A.; Nyamato, G.S.; Ojwach, S.O. Ethylene oligomerization reactions catalyzed by homogeneous and silica immobilized NO Fe (II) and Co (II) complexes. *J. Organomet. Chem.* **2019**, *903*, 120987. [[CrossRef](#)]
31. Ngcobo, M.; Ojwach, S.O. Ethylene oligomerization reactions catalyzed by recyclable Fe (II), Ni (II) and Co (II) complexes immobilized on Fe<sub>3</sub>O<sub>4</sub> magnetic nanoparticles. *Mol. Catal.* **2021**, *508*, 111583. [[CrossRef](#)]
32. Akiri, S.O.; Ojwach, S.O. Structural studies and applications of water soluble (phenoxy) imine palladium (II) complexes as catalysts in biphasic methoxycarbonylation of 1-hexene. *J. Organomet. Chem.* **2021**, *942*, 121812. [[CrossRef](#)]
33. Ngubane, N.P.; Akiri, S.O.; Omondi, B.; Ojwach, S.O. Syntheses of N<sup>o</sup>-donor palladium (II) complexes and applications as recyclable catalysts in biphasic methoxycarbonylation of alkenes. *Polyhedron* **2023**, *237*, 116387. [[CrossRef](#)]
34. Rossetto, E.; Caovilla, M.; Thiele, D.; de Souza, R.F.; Bernardo-Gusmão, K. Ethylene oligomerization using nickel-β-diimine hybrid xerogels produced by the sol–gel process. *Appl. Catal. A Gen.* **2013**, *454*, 152–159. [[CrossRef](#)]
35. Standfest-Hauser, C.M.; Lummerstorfer, T.; Schmid, R.; Hoffmann, H.; Kirchner, K.; Puchberger, M.; Trzeciak, A.M.; Mieczyska, E.; Tylus, W.; Ziółkowski, J.J. Rhodium phosphine complexes immobilized on silica as active catalysts for 1-hexene hydroformylation and arene hydrogenation. *J. Mol. Catal. A Chem.* **2004**, *210*, 179–187. [[CrossRef](#)]
36. Firuzabadi, F.D.; Asadi, Z.; Panahi, F. Immobilized NNN Pd-complex on magnetic nanoparticles: Efficient and reusable catalyst for Heck and Sonogashira coupling reactions. *RSC Adv.* **2016**, *6*, 101061–101070. [[CrossRef](#)]
37. Veisi, H.; Hemmati, S.; Safarimehr, P. In situ immobilized palladium nanoparticles on surface of poly-methyl dopa coated-magnetic nanoparticles (Fe<sub>3</sub>O<sub>4</sub>@PMDA/Pd): A magnetically recyclable nanocatalyst for cyanation of aryl halides with K<sub>4</sub>[Fe(CN)<sub>6</sub>]. *J. Catal.* **2018**, *365*, 204–212. [[CrossRef](#)]
38. Zhang, F.; Jin, J.; Zhong, X.; Li, S.; Niu, J.; Li, R.; Ma, J. Pd immobilized on amine-functionalized magnetite nanoparticles: A novel and highly active catalyst for hydrogenation and Heck reactions. *Green Chem.* **2011**, *13*, 1238–1243. [[CrossRef](#)]
39. Soltani, S.S.; Taheri-Ledari, R.; Farnia, S.M.F.; Maleki, A.; Foroumadi, A. Synthesis and characterization of a supported Pd complex on volcanic pumice laminates textured by cellulose for facilitating Suzuki–Miyaura cross-coupling reactions. *RSC Adv.* **2020**, *10*, 23359–23371. [[CrossRef](#)]
40. Sousa, W.; Guerra, Y.; Peña-García, R.; Padrón-Hernández, E. Saturation magnetization as a function of temperature in Zn doped YIG nanoparticles. *Phys. E Low-Dimens. Syst. Nanostruct.* **2022**, *138*, 115054. [[CrossRef](#)]
41. El Rahman, S.K.A.; Ashour, S.S.; Altass, H.M.; Khairou, K.S. Pd nanoparticles supported on iron oxide nanorods for CO oxidation: Effect of preparation method. *J. Environ. Chem. Eng.* **2016**, *4*, 4794–4800.
42. Yu, L.Q.; Zheng, L.J.; Yang, J.X. Study of preparation and properties on magnetization and stability for ferromagnetic fluids. *Mater. Chem. Phys.* **2000**, *66*, 6–9. [[CrossRef](#)]
43. Sharma, R.K.; Yadav, M.; Gaur, R.; Gupta, R.; Adholeya, A.; Gawande, M.B. Synthesis of iron oxide palladium nanoparticles and their catalytic applications for direct coupling of acyl chlorides with alkynes. *ChemPlusChem* **2016**, *81*, 1312–1319. [[CrossRef](#)] [[PubMed](#)]

44. Verma, S.; Verma, D.; Sinha, A.K.; Jain, S.L. Palladium complex immobilized on graphene oxide–magnetic nanoparticle composites for ester synthesis by aerobic oxidative esterification of alcohols. *Appl. Catal. A Gen.* **2015**, *489*, 17–23. [[CrossRef](#)]
45. Elazab, H.A.; Siamaki, A.R.; Moussa, S.; Gupton, B.F.; El-Shall, M.S. Highly efficient and magnetically recyclable graphene-supported Pd/Fe<sub>3</sub>O<sub>4</sub> nanoparticle catalysts for Suzuki and Heck cross-coupling reactions. *Appl. Catal. A Gen.* **2015**, *491*, 58–69. [[CrossRef](#)]
46. Wang, Z.-J.; Liu, Y.; Shi, P.; Liu, C.-J.; Liu, Y. Al-MCM-41 supported palladium catalyst for methane combustion: Effect of the preparation methodologies. *Appl. Catal. B Environ.* **2009**, *90*, 570–577. [[CrossRef](#)]
47. Mulzer, M.; Whiting, B.T.; Coates, G.W. Regioselective carbonylation of trans-disubstituted epoxides to  $\beta$ -lactones: A viable entry into syn-aldol-type products. *J. Am. Chem. Soc.* **2013**, *135*, 10930–10933. [[CrossRef](#)] [[PubMed](#)]
48. Ma, Y.; Nagy, G.; Siebenbu, M.; Kaur, R.; Dooley, K.M.; Bharti, B. Adsorption and catalytic activity of gold nanoparticles in mesoporous silica: Effect of pore size and dispersion salinity. *J. Phys. Chem. C* **2022**, *126*, 2531–2541. [[CrossRef](#)]
49. Yu, K.; Sommer, W.; Weck, M.; Jones, C.W. Silica and polymer-tethered Pd–SCS–pincer complexes: Evidence for precatalyst decomposition to form soluble catalytic species in Mizoroki–Heck chemistry. *J. Catal.* **2004**, *226*, 101–110. [[CrossRef](#)]
50. Zicarelli, I.; Neumann, H.; Kreyenschulte, C.; Gabriele, B.; Beller, M. Pd-Supported on N-doped carbon: Improved heterogeneous catalyst for base-free alkoxy carbonylation of aryl iodides. *Chem. Commun.* **2016**, *52*, 12729–12732. [[CrossRef](#)]
51. Nakazawa, J.; Doi, Y.; Hikichi, S. Alkane oxidation reactivity of homogeneous and heterogeneous metal complex catalysts with mesoporous silica-immobilized (2-pyridylmethyl) amine type ligands. *Mol. Catal.* **2017**, *443*, 14–24. [[CrossRef](#)]
52. Reynhardt, J.P.; Alper, H. Hydroesterification reactions with palladium-complexed PAMAM dendrimers immobilized on silica. *J. Org. Chem.* **2003**, *68*, 8353–8360. [[CrossRef](#)]
53. Chen, M.; Mou, X.; Wang, S.; Chen, X.; Tan, Y.; Chen, M.; Zhao, Z.; Huang, C.; Yang, W.; Lin, R. Porous organic polymer-supported palladium catalyst for hydroesterification of olefins. *Mol. Catal.* **2020**, *498*, 111239. [[CrossRef](#)]
54. Veisi, H.; Gholami, J.; Ueda, H.; Mohammadi, P.; Noroozi, M. Magnetically palladium catalyst stabilized by diaminoglyoxime-functionalized magnetic Fe<sub>3</sub>O<sub>4</sub> nanoparticles as active and reusable catalyst for Suzuki coupling reactions. *J. Mol. Catal. A Chem.* **2015**, *396*, 216–223. [[CrossRef](#)]

**Disclaimer/Publisher’s Note:** The statements, opinions and data contained in all publications are solely those of the individual author(s) and contributor(s) and not of MDPI and/or the editor(s). MDPI and/or the editor(s) disclaim responsibility for any injury to people or property resulting from any ideas, methods, instructions or products referred to in the content.